ADVANCED FUNCTIONAL MATERIALS
www.afm-journal.de

Superior Micro-Supercapacitors Based on Graphene Quantum Dots

Wen-Wen Liu, Ya-Qiang Feng, Xing-Bin Yan, Jiang-Tao Chen, and Qun-Ji Xue*

Graphene quantum dots (GQDs) have attracted tremendous research interest due to the unique properties associated with both graphene and quantum dots. Here, a new application of GQDs as ideal electrode materials for supercapacitors is reported. To this end, a GQDs//GQDs symmetric micro-supercapacitor is prepared using a simple electro-deposition approach, and its electrochemical properties in aqueous electrolyte and ionic liquid electrolyte are systematically investigated. The results show that the as-made GQDs micro-supercapacitor has superior rate capability up to 1000 V s^{-1}, excellent power response with very short relaxation time constant ($\tau_0 = 103.6$ μs in aqueous electrolyte and $\tau_0 = 53.8$ μs in ionic liquid electrolyte), and excellent cycle stability. Additionally, another GQDs//MnO_2 asymmetric supercapacitor is also built using MnO_2 nanoneedles as the positive electrode and GQDs as the negative electrode in aqueous electrolyte. Its specific capacitance and energy density are both two times higher than those of GQDs//GQDs symmetric micro-supercapacitor in the same electrolyte. The results presented here may pave the way for a new promising application of GQDs in micro-power suppliers and microenergy storage devices.

1. Introduction

Today's rapid growth of portable electronic equipment, wireless sensor networks, and miniaturized electronic devices is driving an increasing demand for micropower sources with small dimensions and high power density.[1,2] Moreover, microscale energy storage units are especially important for integrating energy conversion devices (e.g., piezoelectric nanogenerators,[3] solar cells,[4] and thermoelectric cells[5]) and other electronic circuits, to build self-powered micro/nanodevice systems. However, microbatteries often suffer from fundamental problems caused by the electrochemical reactions. Relatively poor charge/discharge rates and limited cycle life (hundreds to thousands of cycles only) are inevitable in those redox reactions.[6,7]

Supercapacitors, also called electrochemical capacitors, store energy using either electrochemical double layer effect or fast surface redox reactions (pseudocapacitance), which occur at the electrode/electrolyte interface.[1,8] The stored energy mechanisms ensure fast charge and discharge rates (compared with rechargeable batteries) and long cycle life (millions of cycles), and the development of nanomaterials makes supercapacitors keep a reasonable energy density (sometimes even close to that of batteries).[1,8] Due to these advantages, supercapacitors can serve as a major complement to batteries, or even substitute for them, in energy storage and harvesting applications.

Recently, the application of supercapacitors in micropower systems (called as micro-supercapacitors) has become a hot topic for researchers.[9–16] The research efforts mainly focus on enhancing the performances by adjusting the architecture of devices and by improving the capacitive properties of electrode materials. From the device architecture aspect, small-size interdigital finger electrodes have gained more interest in comparison with conventional 2D stacking of thin film electrodes, which is due to two main advantages: i) having two electrodes in the same plane and ii) improved kinetic performance.[15,17] From the electrode material aspect, various nanostructural materials, such as carbon nanotubes (CNTs),[16] activated carbons,[13] carbide derived carbons,[15] onion-like carbon,[14] graphene,[18] ruthenium oxide (RuO_2),[19] manganese dioxide (MnO_2),[20] polypyrrole (PPy),[21] and polyaniline (PANI)[22,23] have been utilized as electrode materials for micro-supercapacitors. However, their performances are still unsatisfactory for the practical application of micro-supercapacitors.

Graphene quantum dots (GQDs), single or few layer graphene with a tiny size of only several nanometers, stand for a new type of quantum dots (QDs) with the unique properties associated with both graphene and QDs.[24] Due to the excellent properties such as high specific surface area, good electrical conductivity, high mobility, tunable band gaps, good biocompatibility, strongle luminescence, and good dispersion in various solvents,[24,25] GQDs have attracted extensive attentions from scientists, and also exhibited bright promise in bio-imaging devices,[26] photovoltaic devices,[27] light-emitting

W.-W. Liu, Y.-Q. Feng, Prof. X.-B. Yan, Dr. J.-T. Chen
Laboratory of Clean Energy Chemistry and Materials
Lanzhou Institute of Chemical Physics
Chinese Academy of Sciences
730000 Lanzhou, P. R. China
E-mail: xbyan@licp.cas.cn
W.-W. Liu, Prof. X.-B. Yan, Prof. Q.-J. Xue
State Key Laboratory of Solid Lubrication
Lanzhou Institute of Chemical Physics
Chinese Academy of Sciences, 730000 Lanzhou, P. R. China
W.-W. Liu
Graduate University of Chinese Academy of Sciences
100080 Beijing, China

DOI: 10.1002/adfm.201203771

diodes,[28] environment field,[29] and fuel cells.[30] However, to our knowledge, the use of GQDs as a kind of electrode material for supercapacitors is rare.

Here, an attempt to use GQDs for high-performance supercapacitors is reported. To achieve this goal, a GQDs//GQDs symmetric micro-supercapacitor and a GQDs//MnO_2 asymmetric micro-supercapacitor are respectively built using controllable electrodeposition on the interdigital finger electrodes. The results show that, as-made GQDs-based micro-supercapacitors display superior electrochemical properties, including exceptionally high rate capability, high frequency response and excellent cycle stability. Among them, the rate capability and frequency response are the best results in the literatures. The encouraging results make GQDs be promising for the next-generation of high-performance micro-supercapacitors.

2. Results and Discussion

2.1. Characterization of GQDs

Figure 1 displays typical characterization results of as-prepared GQDs. The transmission electron microscopy (TEM) images (Figure 1a and Supporting Information Figure S1) and the estimated size distribution (Figure 1c) show fairly uniform GQDs with a size distribution of 1.0–5.4 nm. High-resolution TEM image (Figure 1b) elucidates the 0.37 nm interlayer spacing of GQDs, approximately equal to that of the interlayer spacing of sheets in bulk graphite (0.34 nm).[29,31] AFM observations (Figure 1d,e) reveal highly dispersed GQDs on the silicon substrate with a typical topographic height of 1.0–2.5 nm, indicating that most GQDs consist of ca. 1–4 graphene layers.[30] The formation of GQDs is further confirmed by UV-vis and photoluminescence (PL) spectra. As shown in **Figure 2**b, the as-prepared GQDs-*N*,*N*-dimethylformamide (DMF) solution exhibits a homogeneous phase without any noticeable precipitation even after several weeks at room temperature. The GQDs-DMF solution excited by a 365 nm lamp (6 W) emits an intense blue-green luminescence (Figure 1f, inset), which is likely attributable to the effect of size and surface functional groups. It is noteworthy that the UV-vis absorption spectrum of the GQDs shows a typical absorption peak around 227 nm due to the $\pi \rightarrow \pi^*$ transition of aromatic sp^2 domains,[28,32] and a long tail extending into the visible range. The GQDs also have another absorption (shoulder) peak centered at a wavelength of 360 nm, which is attributed to the $n \rightarrow \pi^*$ transitions of C=O.[33] The most distinctive feature of GQDs which sets them apart from other previously reported carbon dots is the specific PL. As seen in Figure 1f, on excitation near the absorption band of 365 nm, the PL spectrum shows a strong peak at 480 nm, which is consistent with the reported result.[34]

2.2. Symmetric Micro-Supercapacitor

The electrophoretic deposition of GQDs on the interdigital finger electrodes to prepare GQDs//GQDs symmetric micro-supercapacitor is achieved as shown schematically in Figure 2a. Details on the experimental and schematic process are described in experiment section. It is interesting to note

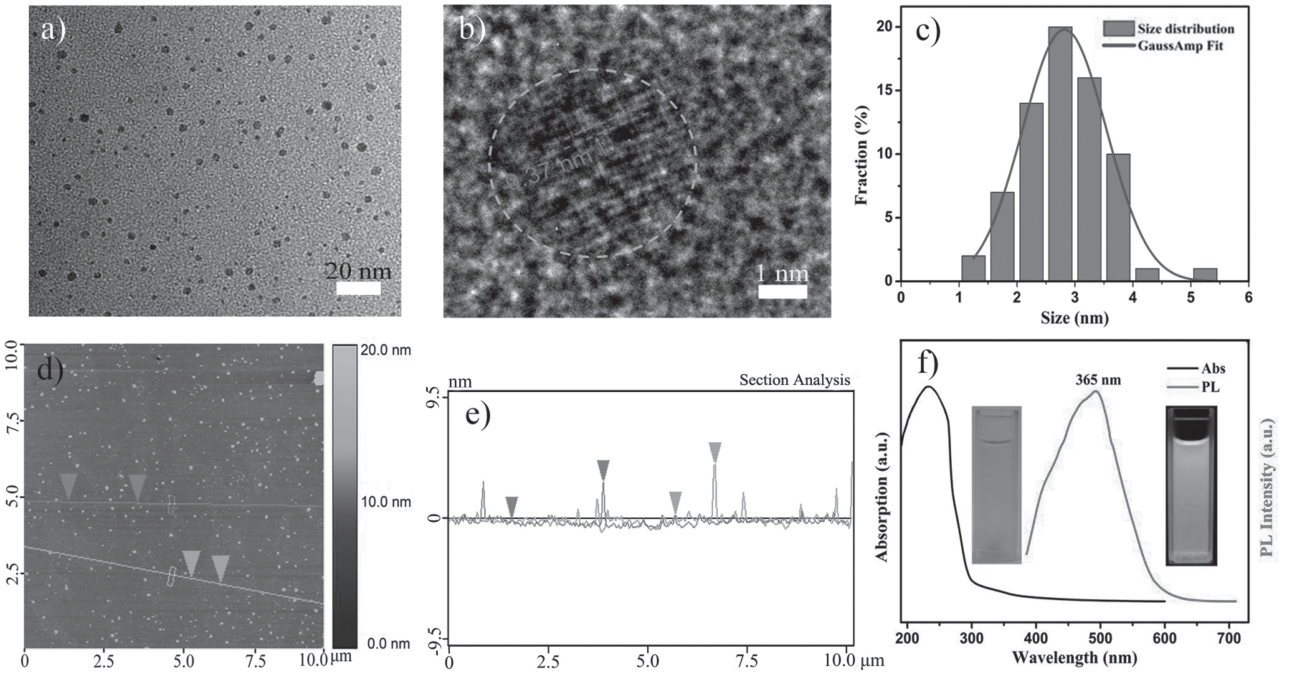

Figure 1. a) TEM images of as-prepared GQDs, b) high-resolution TEM image of an individual GQD, c) the corresponding size distribution of GQDs shown in (a), d) AFM image of GQDs on a single-crystalline silicon wafer substrate, e) the corresponding height profile along the line shown in (d), and f) UV-vis (black line) and PL (red line) spectra of GQDs in DMF at the 365 nm. The insets show the digital photographs of the GQDs in DMF exposed to visible light (left) and ultraviolet light (right).

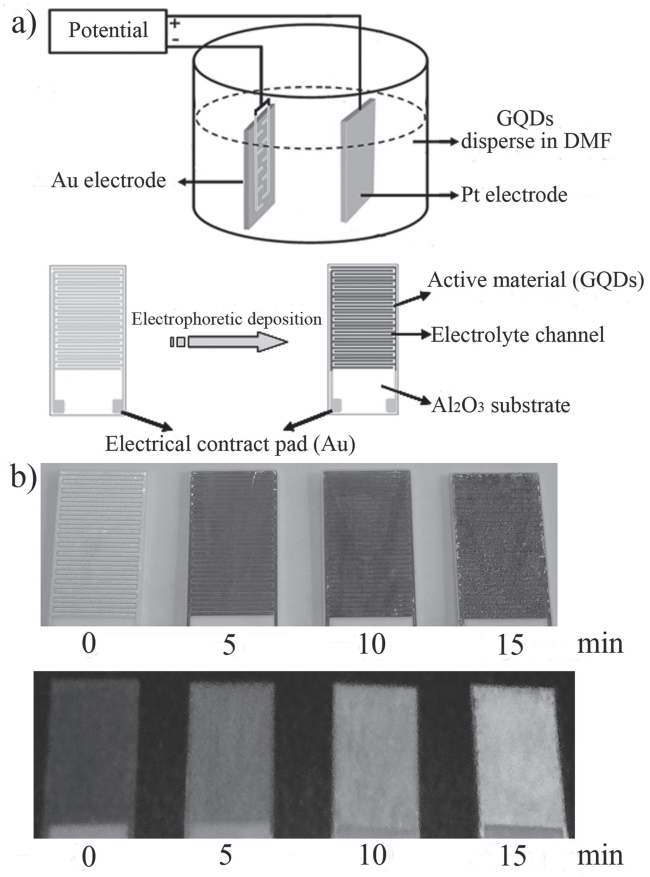

Figure 2. a) Schematic illustration of the electrophoretic deposition of GQDs on the interdigital finger electrodes to prepare a GQDs//GQDs symmetric micro-supercapacitor, b) The digital photographs of the GQDs electrodes with different electro-deposition times exposed to visible light (top) and ultraviolet light (bottom).

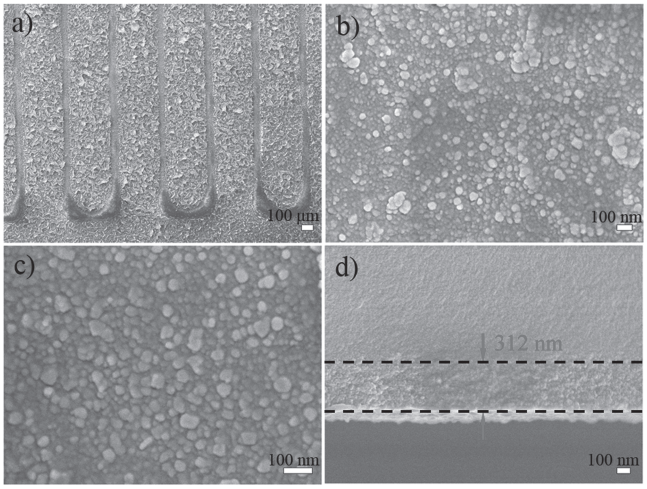

Figure 3. SEM images of the interdigital finger electrodes after the deposition of GQDs: a–c) top-view images of two Au electrodes coated with GQDs with different magnifications and d) cross-section image of an Au electrode finger coated with GQDs.

that, the microelectrodes emit different colors under UV irradiation by a 365 nm lamp after the deposition of GQDs, and the color changes from purple to blue with the increase of deposition time (Figure 2b). The results suggest the successful preparation of GQDs coating on the interdigital finger electrodes by the electrophoretic deposition (EPD) technology.

The micro-supercapacitor consists of 32 in-plane interdigital Au microelectrodes (16 positive and 16 negative microelectrodes). Each microelectrode is 230 μm in width and 10 mm in length, and the distance between adjacent microelectrodes is 200 μm. **Figure 3**a shows the scanning electron microscopy (SEM) image of a piece of the planar interdigital finger micro-supercapacitor device, which reveals that the GQDs form a relatively uniform coating on the Au substrate. The SEM image at high magnification (Figure 3b,c) reveals that the deposited GQDs gather together to form nanoparticles. Figure 3d shows the cross-sectional SEM image of the Au microelectrode coated with GQDs. No obvious defect or pores are observed at the interlayer between the Au-electrode collector and the GQDs layer, indicating the good adhesion. The thickness of the GQDs layer is around 312 nm, which can be easily controlled by adjusting the deposition time. In addition, the microstructure changes of GQDs after the EPD are investigated by X-ray diffraction (XRD) and Fourier transform infrared (FTIR; see Supporting Information Figure S2). In comparison, there is no difference between the as-made powdery GQDs and the collected GQDs from the electrodeposited GQDs coating, demonstrating that the EPD process has negligible influence on the intrinsic crystallinity and carbon-carbon conjugated backbones of GQDs.

The electrochemical behavior of as-made GQDs//GQDs symmetric micro-supercapacitor is firstly analyzed by cyclic voltammetry (CV) at scan rates from 0.02 V s^{-1} to 1000 V s^{-1}. As shown in **Figure 4**a,b, the CV curves of the GQDs//GQDs symmetric micro-supercapacitor keep the typical rectangular in shape when the scan rate increases from 1 V s^{-1} to 100 V s^{-1}, which represents an ideal capacitive behavior.[35,36] Importantly, even at a very high scan rate of 1000 V s^{-1} (Figure 4c), the CV curve still maintains the rectangular in shape without any variance, indicating a fast charge transfer in the bulk of the GQDs and a small equivalent series resistance (ESR) of the micro-supercapacitor.[37,38] Such GQDs//GQDs symmetric micro-supercapacitor has much better rate performance compared with the interdigital structural micro-supercapacitors based on other nanomaterials, including carbide-derived carbon,[15] onion-like carbon,[14] the electrochemical reduction of graphene oxide (ErGO),[37] reduced graphene oxide (rGO)-carbon nanotube (CNT) composites,[36] polyaniline (PANI),[22] polypyrrole (PPy),[39,40] MnO_2,[20,41] and RuO_2.[10] In addition, it can be observed that the nearly linear increase of the charge current densities for the GQDs//GQDs symmetric micro-supercapacitor at 0.5 V with the scan rates ranging from 0.02 V s^{-1} to 1000 V s^{-1} (Figure 4d), indicating its high power output capability due to the fast diffusion of electrolyte and the fast charge transport.[42] To the best of our knowledge, this up-limit of scan rate (1000 V s^{-1}) for the linear relationship is the highest among all reported micro-supercapacitors based on other types of active materials, including the ErGO,[37] carbon fiber (CF)-MnO_2 composites,[42] and silicon nanowire (SiNW).[43] The

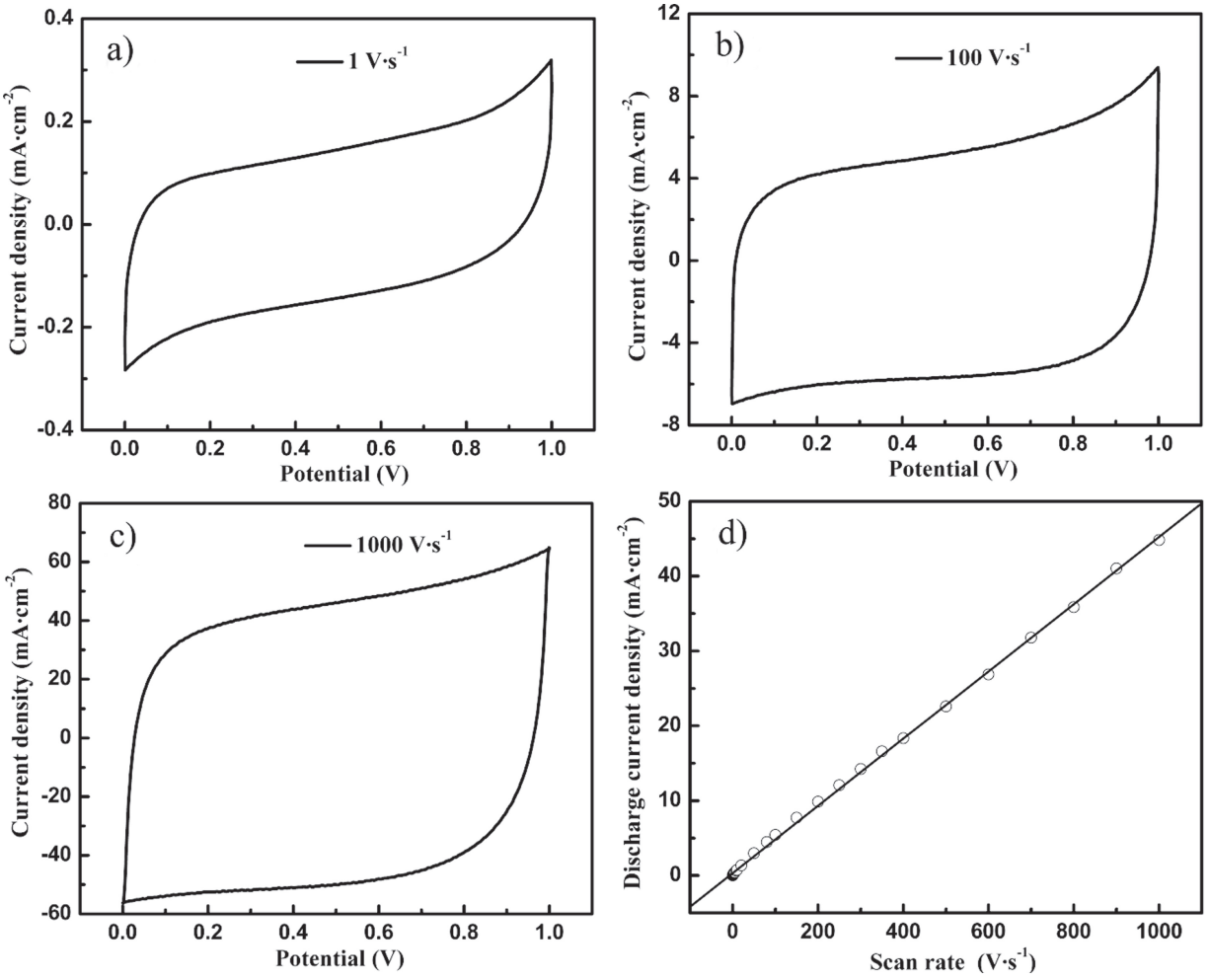

Figure 4. CV curves of GQDs//GQDs symmetric micro-supercapacitor obtained in 0.5 M Na_2SO_4 electrolyte at different scan rates: a) 1 V s^{-1}, b) 100 V s^{-1}, and c) 1000 V s^{-1}. d) The relationship between the charge current densities and the scan rates at 0.5 V.

reasons for the excellent CV performance of GQDs are as follows. First, compared with graphene sheets, GQDs have larger specific surface area, more surface active sites, and more accessible edges, which can conveniently afford ample interfaces for the fully accessible of ion adsorption/desorption. Second, compared with other active materials (carbon materials excepting graphene sheets, metal oxides and conductive polymer), GQDs can be regarded as quantum sized graphene fragments. The excellent electron mobility of GQDs is favorable to increase the conductivity of the active layer and greatly facilitate the charge transport through the active layer.

Electrochemical impedance spectrometry (EIS) is performed to further evaluate the electrochemical performance of GQDs// GQDs symmetric micro-supercapacitor. For an ideal electrical double-layer capacitor (EDLC), the low frequency region of its Nyquist plot is a straight line. The more vertical the line, the more closely the supercapacitor behaves as an ideal capacitor.[44,45] According to the EIS measurement, the straight line nearly parallels to the imaginary axis at the low frequency region (**Figure 5**a), revealing an ideal capacitive behavior related to the charging/discharging mechanism of GQDs film.[46] Also, the plot does not show a semicircle at the high frequency region, implying the fast charge transfer in the bulk of GQDs related to interfacial processes.[46] The ESR value deduced from the point of the curve interaction with lateral axis is about 1.35 Ω. In general, the power output capability of electrochemical supercapacitors depends strongly on not only the rate of ionic mass transport but also the ESR.[47,48] Therefore, the superior rate performance for GQDs//GQDs symmetric micro-supercapacitor may be also attributed to its relatively small ESR.

For a more informative analysis of EIS test, the dependence of phase angle on the frequency of the micro-supercapacitor is plotted in Figure 5b. It is known that the closer the phase angle approaches 90°, the more excellent capacitor behavior the device has.[37] In the case of the GQDs//GQDs micro-supercapacitor, a very small arc is observed in the high-frequency region (Figure 5a), suggesting that the electronic resistance between GQDs and Au current collector should be small. At lower frequencies, a vertical line close to 90° is observed, and a simple response that can be approximately regarded as an

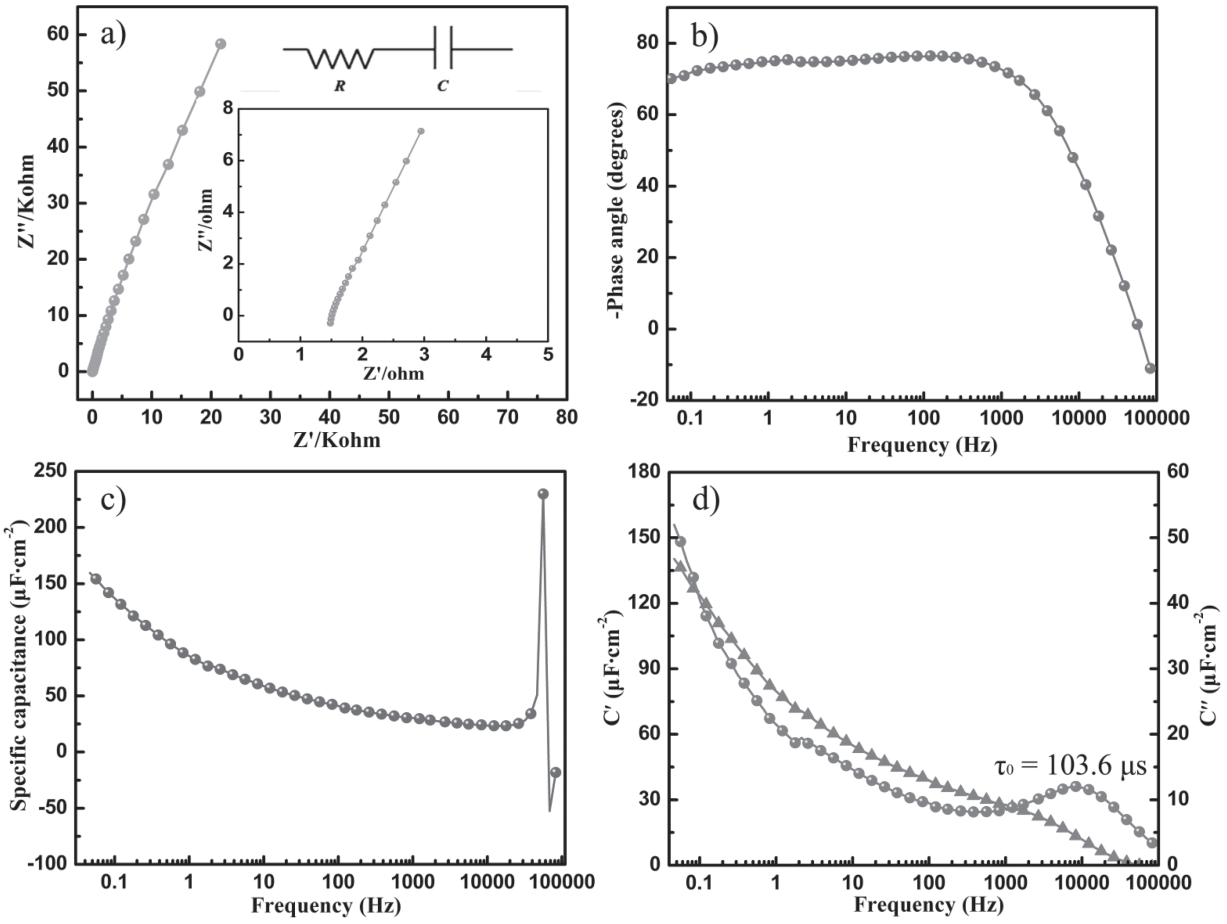

Figure 5. a) Nyquist plot of GQDs//GQDs symmetric micro-supercapacitor, b) plot of impedance phase angle versus frequency, c) plot of specific capacitance versus frequency using a series-RC circuit model, and d) plot of the real or imaginary part (C′ or C″) of specific capacitance versus frequency. The inset of (a) is an expanded view in the region of high frequencies and an equivalent circuit model.

ideal capacitive behavior without a wide distribution of R and C.[49] These results demonstrate that ionic diffusion is not a rate-determining process in the GQDs//GQDs micro-supercapacitor and there is no wide dispersion of resistances and capacitances in the electrodes' structures.[49] This means that there is an almost unique resistor-capacitor (RC) time constant or a capacitance connected with a bulk resistance in series, as shown inset of Figure 5a. Consequently, a series RC circuit model is used to stimulate the capacitive and resistive elements of the GQDs//GQDs symmetric micro-supercapacitor.[50] In this model, resistance is the real part of impedance spectrum, and the capacitance (C) is calculated by using the equation of $C = (-1)/(2\pi fZ'')$, where f is the frequency in Hz and Z'' is the imaginary part of the impedance spectrum.[49] C_s is defined as C/S (where C is the capacitance and S is the apparent surface area of the electrode). In our system, S is calculated to be 0.368 cm^2. As shown in Figure 5c, theC_s increases from 25.0 μF cm^{-2} to 160.1 μF cm^{-2} as the frequency decreases from 10 KHz to 0.05 Hz. In addition, compared with the C_s value of GQDs//GQDs symmetric micro-supercapacitor (160.1 μF cm^{-2}) at 0.05 Hz, the C_s of the bare interdigital structure Au electrode is only 7.8 μF cm^{-2} at 0.05 Hz (see Supporting Information Figure S3). Thus, it is reasonable to conclude that the C_s of GQDs//GQDs symmetric micro-supercapacitor is mainly attributed to the contribution of GQDs active material. Furthermore, a further comparison of the frequency response of the micro-supercapacitor can be made by comparing the characteristic frequency (f_0) which is the frequency at a phase angle of 45° or its corresponding relaxation time constant ($\tau_0 = 1/f_0$).[36] The characteristic frequency marks the point at which the resistive and capacitive impedance are equal and at frequencies higher than f_0 supercapacitors shows a more resistive behavior.[51,52] The corresponding relaxation time constant (τ_0) is the minimum time needed to discharge all the energy from the device with an efficiency of greater than 50%,[14,36] and it can be derived from the frequency at the peak capacitance of C''. It can be observed that both the impedance phase angle of the micro-supercapacitor reaching 45° (Figure 5b) and the peak capacitance of C'' (Figure 5d) appear at about 9651 Hz (τ_0 = 103.6 μs), and this frequency is much higher than those of reported high-rate supercapacitors based on activated carbon at 1.4 Hz (τ_0 = 714 ms),[14] rGO at 30.3 Hz (τ_0 = 33 ms),[36] onion-like carbon at 38.5 Hz (τ_0 = 26 ms),[14] carbon fibers-MnO_2 at 45.4 Hz (τ_0 = 22 ms),[38] rGO-CNT at 291 Hz (τ_0 = 3.4 ms),[36] CNTs at 1172 Hz

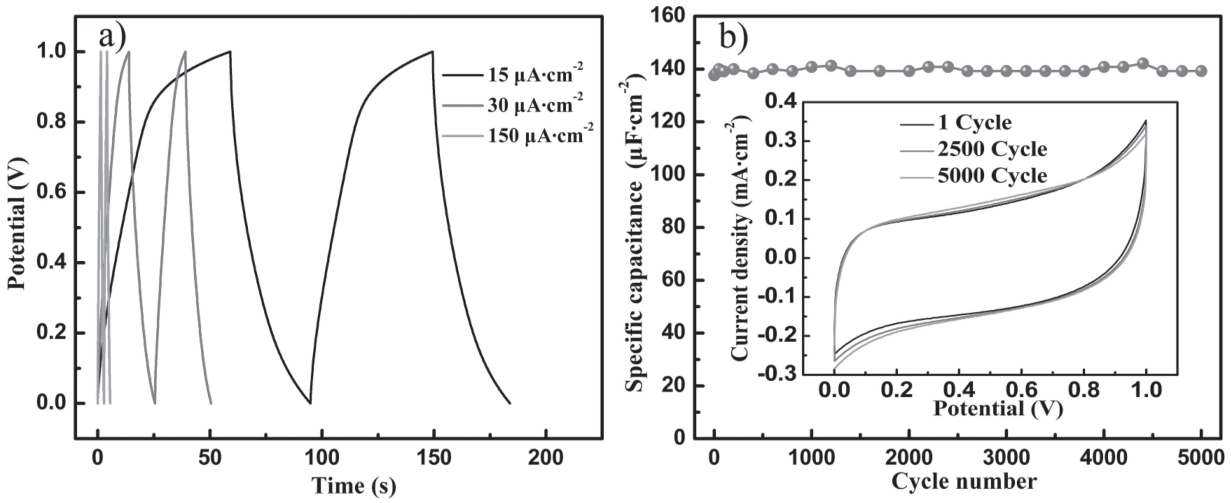

Figure 6. a) GCD curves of GQDs//GQDs symmetric micro-supercapacitor at the different current densities of 15, 30, and 150 μA cm^{-2}. b) The specific capacitance as a function of cycle number measured at 1 V s^{-1} in 0.5 M Na_2SO_4 aqueous solution. Inset is the CV curves of the 1st, 2500th and 5000th cycles.

(τ_0 = 0.85 ms),[53] and ErGO at 4202 Hz (τ_0 = 0.24 ms).[37] The extremely small corresponding relaxation time constant (τ_0 = 103.6 μs) reveals the excellent power response of the GQD// GQD symmetric micro-supercapacitor.

As shown in **Figure 6**a, the GCD curves of GQDs//GQDs symmetric micro-supercapacitor at different current densities are near triangle-shaped curves, further verifying that it has high reversibility and ideal capacitor behavior mainly originating from the electric double layer at the GQDs film/electrolyte interface.[54] It should be noted that the slightly asymmetric charge/discharge curve at low current density of 15 μA cm^{-2} is due to the contribution from the pseudocapacitance taking place at the electrode/electrolyte interface. Generally, a redox reaction will take longer time than pure electric double layer formation.[55] At a low current density, the side-reactions have the enough time to take place at the electrode/electrolyte interface during the charge/discharge process. So there is a competition between the double layer formation and the side-reactions, which results in the slightly asymmetric charge/discharge curves.[55,56] No obvious IR drop is observed on the start of all discharge curves, elucidating that GQDs//GQDs symmetric micro-supercapacitor bears a relatively small internal series resistance.[54,57] As pointed out by Gogotsi and Simon,[58] the areal capacitance or energy density are much more reliable performance metrics for supercapacitor devices compared to gravimetric capacitance. This is more pronounced in the case of micro-supercapacitor as the weight of the active material (GQDs) is negligible. Thus, all of the C_s of the micro-supercapacitors are evaluated in area units (μF cm^{-2}), if not otherwise specified. The GQDs//GQDs symmetric micro-supercapacitor shows the specific capacitor of 534.7 μF cm^{-2} and the energy density of 0.074 μWh cm^{-2} (with the specific power of 7.5 μW cm^{-2} at this point) at the current density of 15 μA cm^{-2}. The results are better than the reported values of graphene-based film supercapacitor and micro-supercapacitors, such as the CVD graphene nanosheets (80 μF cm^{-2}),[59] reduced multilayer GO (394 μF cm^{-2}),[59] ErGO (487 μF cm^{-2}),[37] and RGO-GO-RGO supercapacitor devices (510 μF cm^{-2}).[60]

The cycle stability of supercapacitors is an important parameter to evaluate its potential for practical applications.[61] Figure 6b shows the change of the specific capacitance as the number of cycles increases, obtained from the CV test at a scan rate of 1 V s^{-1}. The micro-supercapacitor displays an approximately 97.8% retention of its initial specific capacitance after 5000 continuous cycles, which is comparable to that of other active materials including ErGO (99% retention after 10 000 cycles),[37] CNT-based stretchable supercapacitor (98.5% retention after 1000 cycles),[62] laser-scribed graphene electrochemical capacitors (96.5% retention after 10000 cycles),[63] rGO-CNT micro-supercapacitors (95% retention after 1000 cycles),[36] and rGO/PANI composite (90% retention after 1700 cycles).[23] This result indicates that the GQDs//GQDs symmetric micro-supercapacitor possesses good long-term electrochemical stability.

Since the specific energy of a supercapacitor is proportional to the square of the operating voltage ($E_{max} = ½CV^2$), it remains a challenge to achieve high energy in aqueous media due to the low decomposition voltage limit of water (around 1.2 V).[64] In this sense, organic electrolytes or ionic liquids dissolved in propylene carbonate or acetonitrile (AN), allowing to operate the voltages of typically 2.5–2.7 V, have been employed in many commercial supercapacitors specially oriented to higher energy applications.[65,66] Herein, to extend the voltage window of our micro-supercapacitor, 1-ethyl-3-methylimidazolium tetrafluoroborate ($EMIMBF_4$) ionic liquid, is chosen as the electrolyte, which has been widely used as electrolyte in commercial EDLCs. As shown in **Figure 7**a–d, the CVs of GQDs in 2 M $EMIMBF_4$/AN also exhibits a nearly rectangular-shaped pattern and a linear dependence between the charge current densities and the scan rates. It is indicative of nearly ideal capacitive behavior of the micro-supercapacitor in ionic liquid electrolyte.

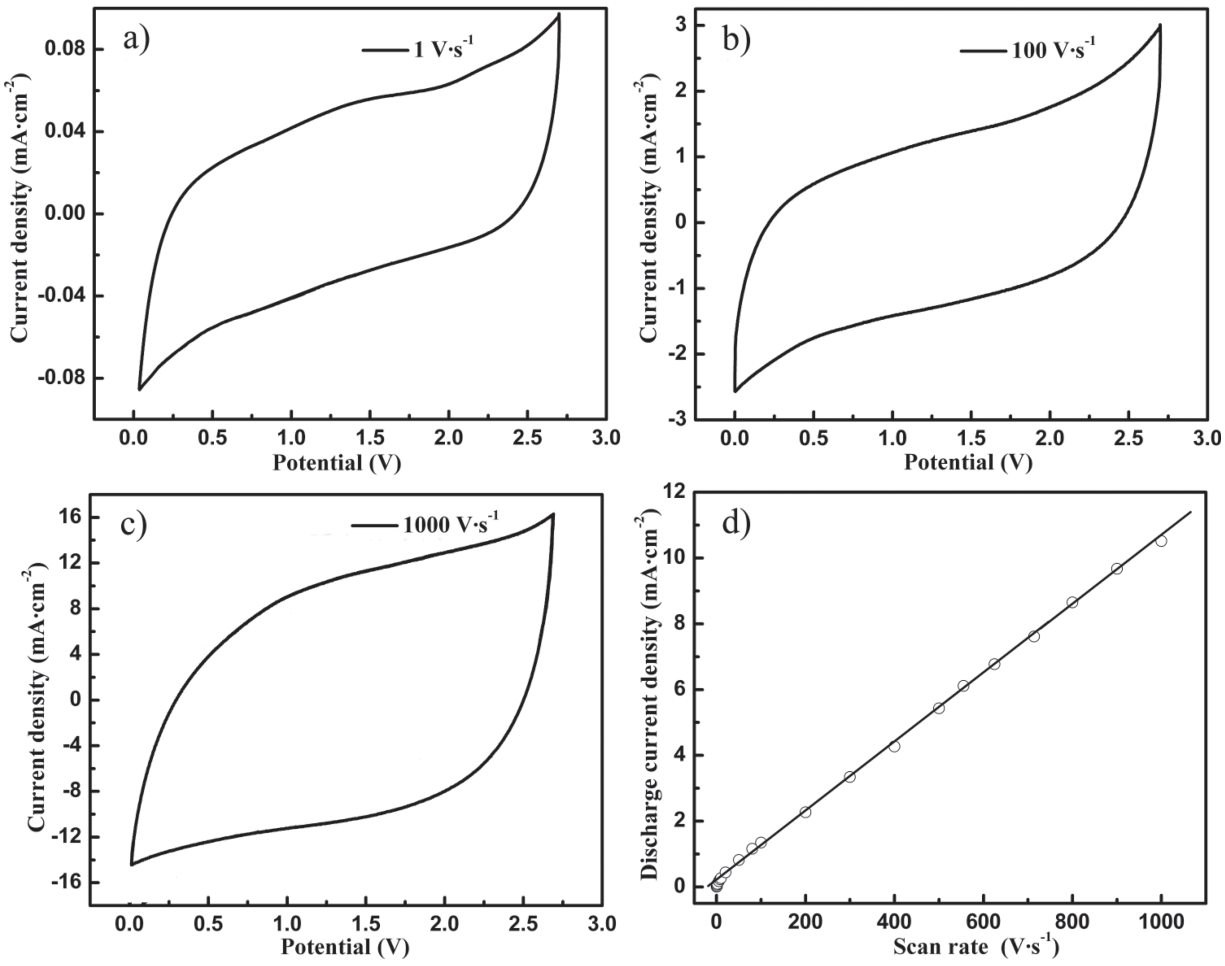

Figure 7. CV curves of GQDs//GQDs symmetric micro-supercapacitor obtained in 2.0 M $EMIMBF_4$/AN electrolyte at different scan rates: a) 1 V s^{-1}, b) 100 V s^{-1}, and c) 1000 V s^{-1}. d) The relationship between the charge current densities and the scan rates at 1.35 V.

However, the CVs in 2 M $EMIMBF_4$/AN electrolyte show a slower current response at the switching potentials (0 V and 2.7 V) compared with that in 0.5 M Na_2SO_4 aqueous electrolyte. A likely reason for this difference is that the $EMIMBF_4$/AN has the relatively high viscosity,[67,68] resulting in the slow re-organization of the double layer at the GQDs and $EMIMBF_4$/AN electrolyte interlayer.

The GCD and EIS measurements are also carried out to investigate the performances of the micro-supercapacitor in $EMIMBF_4$/AN electrolyte. The triangle-shaped GCD curves (**Figure 8**a) and the phase angle approaching 75° (Figure 8b) demonstrate the typical capacitor behavior.[37] The symmetric micro-supercapacitor in $EMIMBF_4$/AN electrolyte shows the specific capacitance of 468.1 μF cm^{-2} and the energy density of 0.474 μWh cm^{-2} (with the specific power of 56.7 μW cm^{-2} at this point) at the current density of 15 μA cm^{-2}. The energy density and power density are about seven times higher than those in Na_2SO_4 aqueous electrolyte. The impedance phase angle of the micro-supercapacitor up to 45° (Figure 8b) is at about 18,588 Hz (τ_0 = 53.8 μs), demonstrating faster frequency response of the GQDs//GQDs symmetric micro-supercapacitor in ionic liquid electrolyte than that in aqueous electrolyte. Moreover, as shown in Figure 8c, theC_s of the micro-supercapacitor increases from 7.5 to 60.7 μF cm^{-2} as the frequency decreases from 100 KHz to 0.05 Hz. Additionally, its capacitance decays only 6% of its initial specific capacitance after 5000 cycles even at a scan rate of 1 V s^{-1} (Figure 8d), exhibiting the excellent cycle life of GQDs//GQDs symmetric micro-supercapacitor in ionic liquid electrolyte.

2.3. Asymmetric Supercapacitors

Because of having higher energy and power densities than carbon materials in aqueous electrolytes, metal oxides have been explored as a kind of electrode material for pseudocapacitors. Among numerous metal oxides, manganese dioxide (MnO_2) is considered to be a most attractive candidate as electrode material for supercapacitors because of its abundant natural resources, low-cost, environmental friendliness, and high specific capacitance.[69] Herein, a GQDs//MnO_2 asymmetric micro-supercapacitor (**Figure 9**a), based on the redox character of MnO_2 and the electric double-layer storage of GQDs, is successfully fabricated as well. As shown in Figure 9b, the dark

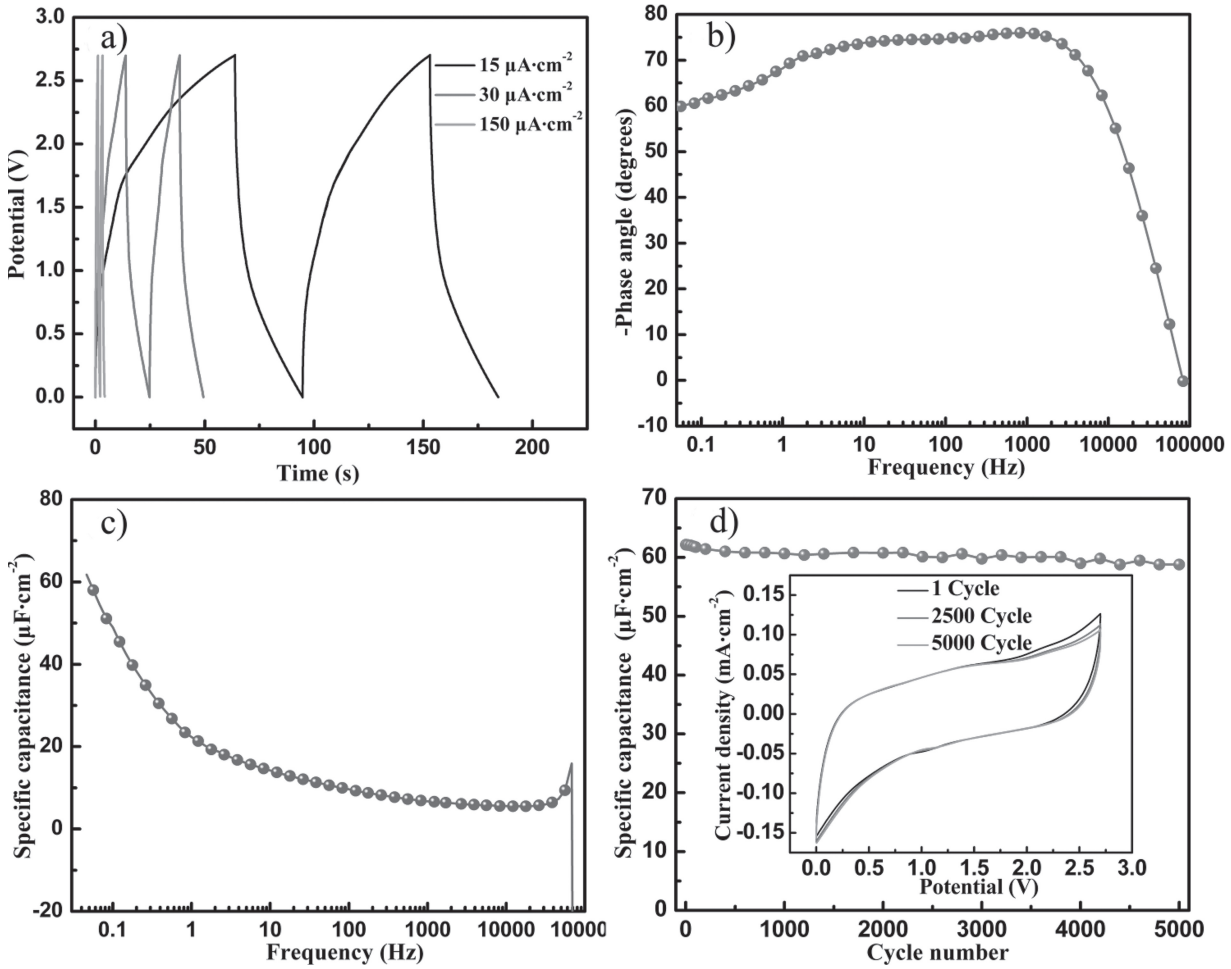

Figure 8. a) GCD curves of GQDs//GQDs symmetric micro-supercapacitor obtained in 2.0 M $EMIMBF_4$/AN electrolyte at the different current densities of 15, 30, and 150 μA cm^{-2}, b) plot of impedance phase angle versus frequency, c) plot of specific capacitance versus frequency using a series-RC circuit model, and d) the specific capacitance as a function of cycle number cycle measured at 1 V s^{-1}. Inset is the CV curves of the 1st, 2500th and 5000th cycles.

region in the SEM image represents the negative active material of GQDs, while the light region represents the positive active material of MnO_2. It is interesting to note that the as-prepared MnO_2 has similar structure with that of pine branch, an ornamental evergreen tree that is native to northeast Asia (inset of Figure 9c). The individual pine-branch shaped MnO_2 is micro-sized and is composed by many MnO_2 nanoneedles with the diameter of 5–10 nm and the length up to 50 nm (Figure 9d). Moreover, a lot of mesopores present among these nanoneedles, which are beneficial to reduce the diffusion path of ions. In addition, XRD pattern and FTIR spectrum (see Supporting Information Figure S4) exhibit that the obtained MnO_2 is γ-MnO_2, a random intergrowth of two types of structural units: pyrolusite (1 × 1 channels) and ramsdellite (1 × 2 channels),[70] which allows the reversible insertion/extraction of alkali cations through the bulk of the MnO_2 material.[71]

To evaluate the electrochemical properties of GQDs//MnO_2 asymmetric micro-supercapacitor, CV, GCD and EIS measurements are carried out in 0.5 M Na_2SO_4 electrolyte. It can be clearly seen that, as the scan rate increases from the 1 V s^{-1} to 100 V s^{-1} (**Figure 10**a,b), the CV curves shows a relatively ideal rectangular in shape and near mirror-image current response on voltage reversal, and no obvious redox peak is observed, indicating an ideal capacitive behavior.[72] Importantly, even at a high scan rate of 1000 V s^{-1} (Figure 10c), the CV curve still remains quasi-rectangular in shape, suggesting the excellent reversibility of electrode process. It is mainly attributed to the unique structure of γ-MnO_2 which is benefited to the movement of electrolyte ions.

Figure 11a shows the GCD curves of GQDs//MnO_2 asymmetric supercapacitor at different current densities. An approximate linear relationship of the charge/discharge potentials with time is found, indicating a rapid current density–voltage (*I*–*V*) response and small ESR.[72] Moreover, it can be observed that the discharge curve is nearly symmetric with its corresponding charging counterpart, demonstrating the excellent electrochemical reversibility and good coulombic efficiency.[72] The GQDs//MnO_2 asymmetric micro-supercapacitor shows the specific capacitance of 1107.4 μF cm^{-2} and the energy density of 0.154 μWh cm^{-2} (with the specific power of 7.51 μW cm^{-2} at this point) at the current density of 15 μA cm^{-2}. This energy density

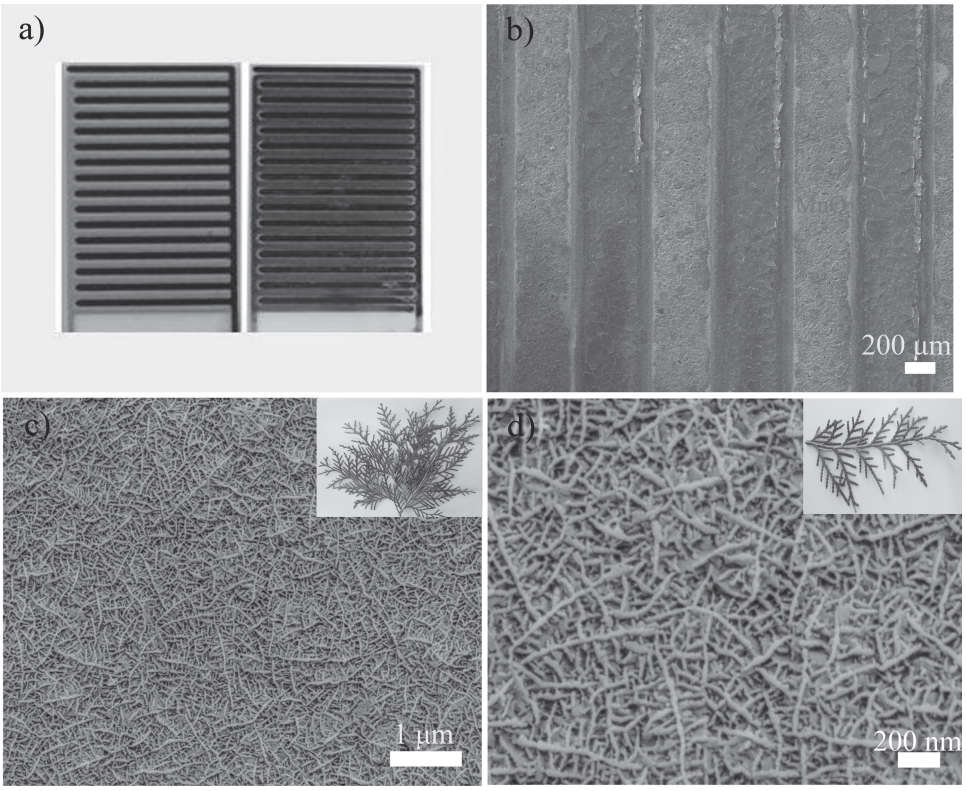

Figure 9. a) Digital photographs of GQDs//MnO_2 asymmetric micro-supercapacitor built by the electro-deposition of the MnO_2 (right), and then deposited the GQDs (left), b) SEM image of the interdigital finger electrodes after the deposition of GQDs and MnO_2, and c,d) top-view SEM images of MnO_2 coating with low and high magnifications. The insets are photographs of a kind of pine branches native to northeast Asia.

is two times higher than that of GQDs//GQDs symmetric micro-supercapacitor, and it is mainly attributed to the pseudo-capacitance contribution of MnO_2. As seen in Figure 11b, the phase angle is about 66° at 0.05 Hz, indicating a good capacitor behavior of the asymmetric supercapacitor device. In addition, the supercapacitor shows about 93.3% retention of its initial specific capacitance after 5000 cycles between 0 V and 1.0 V at a scan rate of 1 V s^{-1} (Figure 11c), indicating good cycle stability. The slight decay of specific capacitance may be attributed to an irreversible mass loss caused by low dissolution and slow diffusion of active MnOOH during cycling process or the loss of adhesion of some active material with the current collector.[73] The superior electrochemical performances of GQDs//MnO_2 asymmetric micro-supercapacitor can be reasonably attributed to the synergistic effects between the positive and negative electrodes. On the one hand, GQDs electrode in the asymmetric supercapacitor still maintain the distinctive features such as the good electrochemical stability and superior conductivity. On the other hand, γ-MnO_2 electrode facilitates the transport of electrolyte ions and provides abundant surfaces for charge-transfer reactions.

3. Conclusions

In summary, through fabricating GQDs-based micro-supercapacitors and studying their electrochemical properties, a new application of GQDs as an electro-active material for supercapacitors is identified. The electrochemical tests show that as-made GQDs//GQDs symmetric micro-supercapacitor has superior rate capability with the scan rate up to 1000 V s^{-1}, excellent power response with a small RC time constant (103.6 μs), high area specific capacitor (468.1 μF cm^{-2}), and outstanding cycle stability in 0.5 M Na_2SO_4 aqueous solution. Meanwhile, the GQDs//GQDs symmetric micro-supercapacitor in 2 M EMIMBF_4/AN electrolyte shows a larger voltage window of 2.7 V, a smaller RC time constant (53.8 μs) and a seven times higher energy density compared with that in Na_2SO_4 electrolyte. In addition, another kind of GQDs//MnO_2 asymmetric micro-supercapacitor is also built. Compared with GQDs//GQDs symmetric micro-supercapacitor in aqueous electrolyte, GQDs//MnO_2 asymmetric micro-supercapacitor displays two times higher specific capacitance (1107.4 μF cm^{-2}) and energy density (0.154 μWh cm^{-2}). The excellent supercapacitive performances of GQDs-based micro-supercapacitors are mainly attributed to the unique properties of GQDs such as large specific surface area, abundant active sites and accessible edges. Predictably, the current study probably provides a new direction to explore the energy storage behavior and mechanism of GQDs, and gives a new insight for designing and synthesizing GQDs-based electrode materials for high-performance supercapacitors and other energy-storage devices.

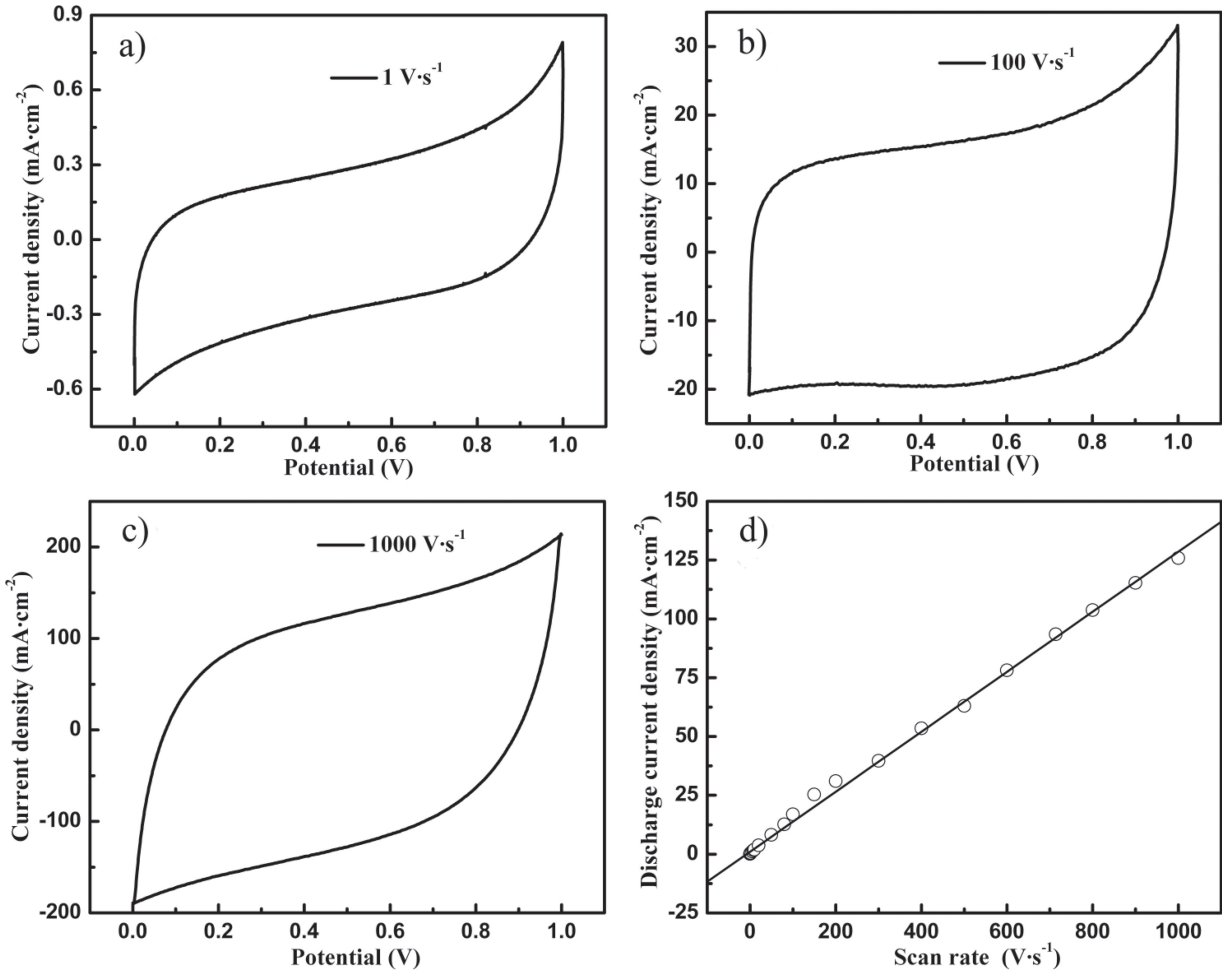

Figure 10. CV curves of GQDs//MnO_2 asymmetric micro-supercapacitor obtained in 0.5 M Na_2SO_4 electrolyte at different scan rates: a) 1 V s^{-1}, b) 100 V s^{-1}, and c) 1000 V s^{-1}. d) The relationship between the charge current densities and scan rates at 0.5 V.

4. Experimental Section

Materials and Chemicals: High-purity graphite powder (99.9%, 325 mesh) was purchased from Qingdao Huatai Tech. Co., Ltd., China. DMF was purchased from Tianjin Reagent Company, China. $EMIMBF_4$ ionic liquid was obtained from the Center for Green Chemistry and Catalysis, Lanzhou Institute of Chemical Physics, Chinese Academy of Sciences. All conventional chemicals were of analytical grade and were used without further purification. Ultrapure water (18 MΩ cm) was used in all experiments.

Fabrication of GQDs: At first, graphite oxide (GO) was prepared from natural graphite powder by a modified Hummers method.[74–77] GQDs were synthesized from GO power by using a facile one-step solvothermal method.[78,79] In a typical synthesis, GO (540 mg) was suspended in

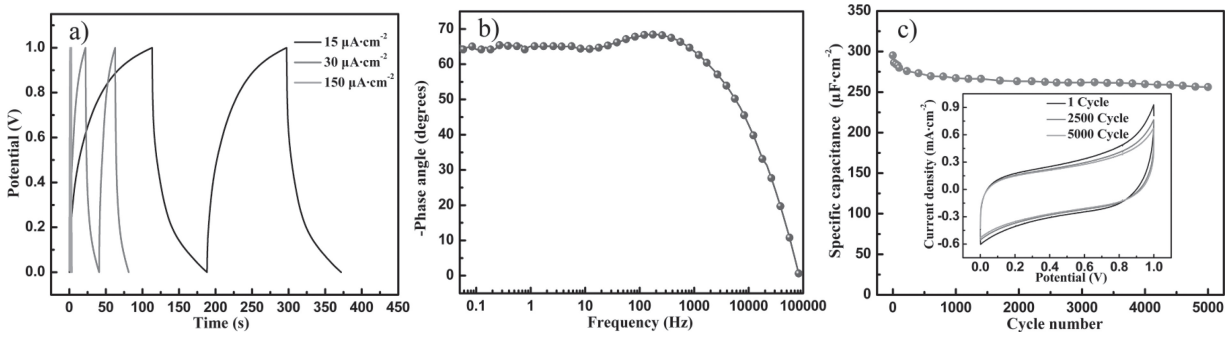

Figure 11. a) GCD curves of GQDs//MnO_2 asymmetric micro-supercapacitor at the different current densities of 15, 30, and 150 μA cm^{-2}, b) plot of impedance phase angle versus frequency, and c) the specific capacitance as a function of cycle number measured at 1 V s^{-1}. Inset is the CV curves of the 1st, 2500th and 5000th cycles.

DMF (40 mL) with the aid of ultrasound (120 W, 40 kHz) for 30 min, and then the suspension was transferred to a poly(tetrafluoroethylene) (Teflon)-lined autoclave (60 mL) and heated up to 200°C for 8 h. After being cooled to room temperature naturally, the mixture was filtered using a 0.22 μm microporous membrane and the brown filter solution was collected, which is the GQDs dispersion in DMF. The dry GQDs powder was obtained by concentrating the brown filter solution with a rotary evaporator at 80°C under reduced pressure.

Preparation of Two Kinds of Micro-Supercapacitors: GQDs//GQDs symmetric micro-supercapacitor was fabricated as follows. Briefly, GQDs were electrodeposited on the interdigital finger Au electrodes in DMF solution (50 mL) containing GQDs (3.0 mg) and $Mg(NO_3)_2$ $6H_2O$ (6.0 mg) at a constant voltage of 80 V for a duration of 30 min. In the electrodeposition system, two Au electrodes connected each other with a Cu wire and a platinum sheet were set as the cathode and the anode, respectively. Subsequently the interdigital finger Au electrodes coated with GQDs were washed with ultrapure water and then dried in air. Figure 2a schematically shows the illustration of the electrophoretic deposition of GQDs on the interdigital finger Au electrodes.

The GQDs//MnO_2 asymmetric micro-supercapacitor was prepared by the following steps. First, GQDs were electrodeposited on one side of the interdigital finger Au electrodes using the above deposition method. Second, MnO_2 was electrochemically deposited on another side of Au electrodes from an electrolyte solution of 0.02 M $Mn(NO_3)_2$ and 0.1 M $NaNO_3$ at a constant current density of 1 mA cm^{-2} with the potential window from −1.2 V to 1.2 V for 5 min. A platinum sheet and an Ag/AgCl electrode were used as the counter and the reference electrodes, respectively (see Supporting Information Figure S5). Finally, the electrodes were washed with ultrapure water and then dried in air.

Morphology and Structural Characterization: TEM investigations were conducted on a JEOL 2100 FEG microscope at 200 keV. SEM analyses were performed on a field emission scanning electron microanalyzer (JEOL-6701F) at 5 kV. XRD patterns of the samples were measured on a powder X-ray diffraction system (XRD, TTR-III) using Cu Ka radiation (k = 0.15406 nm). The AFM image was obtained on a Digital Instrument Nanoscope IIIa AFM (Veeco) in tapping mode. Infrared spectra were recorded on a Varian 3100 FTIR spectrometer by using pressed KBr pellets. UV-vis absorption spectra (Abs) were carried out on a Hitachi U-3010 UV-vis spectrophotometer. PL emission spectra were recorded on an F-4500 fluorescence spectrophotometer.

Electrochemical Measurements: All electrochemical tests, including CV, GCD, and EIS, were carried out in a two-electrode system using an electrochemical working station (CHI660D, Shanghai, China) at room temperature. The CV tests were measured with the potential window from 0 V to 1.0 V for aqueous 0.5 M Na_2SO_4 electrolyte and from 0 V to 2.7 V for organic electrolyte at the scan rates varying from 0.01 V s^{-1} to 1000 V s^{-1}. The GCD tests were measured at different current densities ranging from 15 μm cm^{-2} to 150 μm cm^{-2} (the apparent surface area of each electrode is 0.368 cm^2) in 0.5 M Na_2SO_4 electrolyte and in organic electrolyte, respectively. The EIS measurements were carried out in the frequency range from 0.05 Hz to 100 kHz with 5 mV ac amplitude. The specific capacitance was calculated from the GCD curves based on Equation (1):

$$C = \frac{I\,\Delta t}{A\Delta V}\ (\mu F\ cm^{-2}) \tag{1}$$

The specific energy density and power density were defined according to Equations (2) and (3), respectively:

$$E = \frac{C\Delta V^2}{7200}\ (\mu Wh\ cm^{-2}) \tag{2}$$

$$P = \frac{E\ \ 3600}{\Delta t}\ (\mu W\ cm^{-2}) \tag{3}$$

where I is the current density (μA), Δt is the discharge time (s), ΔV is the potential window of the discharging (V), A is the geometric surface of substrate (cm^{-2}), E is the energy density (μWh cm^{-2}), and P is the energy density (μW cm^{-2}).

Supporting Information

Supporting Information is available from the Wiley Online Library or from the author.

Acknowledgements

This work was supported by the Top Hundred Talents Program of the Chinese Academy of Sciences, the National Nature Science Foundations of China (51005225), and the Youth Science Foundations of Gansu Province (1107RJYA274).

Received: December 19, 2012
Revised: January 21, 2013
Published online: March 26, 2013

[1] C. W. Shen, X. H. Wang, W. F. Zhang, F. Y. Kang, *J. Power Sources* **2011**, *196*, 10465.
[2] Z. Chen, D. Weng, X. L. Wang, Y. H. Cheng, G. Wang, Y. F. Lu, *Chem. Commun.* **2012**, *48*, 3736.
[3] Z. L. Wang, J. H. Song, *Science* **2006**, *312*, 242.
[4] T. S. G. Wee, Y. M. Lam, S. G. Mhaisalkarab, M. Srinivasan, *Energy Environ. Sci.* **2010**, *4*, 413.
[5] C. H. Yu, L. Shi, Z. Yao, D. Y. Li, A. Majumdar, *Nano Lett.* **2005**, *5*, 1842.
[6] J. W. Long, B. Dunn, D. R. Rolison, H. S. White, *Chem. Rev.* **2004**, *104*, 4463.
[7] M. Armand, J. M. Tarascon, *Nature* **2008**, *451*, 652.
[8] P. Simon, Y. Gogotsi, *Nat. Mater.* **2008**, *7*, 845.
[9] H. J. In, S. Kumar, Y. Shao-Horn, G. Barbastathis, *Appl. Phys. Lett.* **2006**, *88*, 083104.
[10] H. X. Ji, Y. F. Mei, O. G. Schmidt, *Chem. Commun.* **2010**, *46*, 3881.
[11] X. Li, B. Q. Wei, *Nano Energy* **2013**, *2*, 159.
[12] W. Sun, R. L. Zheng, X. Y. Chen, *J. Power Sources* **2010**, *195*, 7120.
[13] D. Pech, M. Brunet, P. L. Taberna, P. Simon, N. Fabre, F. Mesnilgrente, V. Conedera, H. Durou, *J. Power Sources* **2010**, *195*, 1266.
[14] D. Pech, M. Brunet, H. Durou, P. H. Huang, V. Mochalin, Y. Gogotsi, P. L. Taberna, P. Simon, *Nat. Nanotechnol.* **2010**, *5*, 651.
[15] J. Chmiola, C. Largeot, P. L. Taberna, P. Simon, Y. Gogotsi, *Science* **2010**, *328*, 480.
[16] M. Kaempgen, C. K. Chan, J. Ma, Y. Cui, G. Gruner, *Nano Lett.* **2009**, *9*, 1872.
[17] M. Beidaghi, C. L. Wang, *Electrochim. Acta* **2011**, *56*, 9508.
[18] H. R. Byon, S. W. Lee, S. Chen, P. T. Hammond, Y. Shao-Horn, *Carbon* **2010**, *49*, 457.
[19] C. B. Arnold, R. C. Wartena, K. E. Swider-Lyons, A. Pique, *J. Electrochem. Soc.* **2003**, *150*, A571.
[20] I. Nam, G. -P. Kim, S. Park, J. Park, N. D. Kim, J. Yi, *Nanoscale* **2012**, *4*, 7350.
[21] W. Sun, X. Y. Chen, *Microelectron. Eng.* **2009**, *86*, 1307.
[22] K. Wang, W. j. Zou, B. G. Quan, A. F. Yu, H. P. Wu, P. Jiang, Z. X. Wei, *Adv. Energy. Mater.* **2011**, *1*, 1068.
[23] M. Q. Xue, F. W. Li, J. Zhu, H. Song, M. N. Zhang, T. B. Cao, *Adv. Funct. Mater.* **2012**, *22*, 1284.
[24] Z. P. Zhang, J. Zhang, N. Chen, L. T. Qu, *Energy Environ. Sci.* **2012**, *5*, 8869.

[25] J. H. Shen, Y. H. Zhu, X. L. Yang, C. Z. Li, *Chem. Commun.* **2012**, *48*, 3686.
[26] S. J. Zhu, J. H. Zhang, C. Y. Qiao, S. J. Tang, Y. F. Li, W. J. Yuan, B. Li, L. Tian, F. Liu, R. Hu, H. N. Gao, H. T. Wei, H. Zhang, H. C. Sun, B. Yang, *Chem. Commun.* **2011**, *47*, 6858.
[27] Y. Li, Y. Hu, Y. Zhao, G. Q. Shi, L. E. Deng, Y. B. Hou, L. T. Qu, *Adv. Mater.* **2011**, *23*, 776.
[28] L. Tang, R. Ji, X. Cao, J. Lin, H. Jiang, X. Li, K. S. Teng, C. M. Luk, S. Zeng, J. Hao, S. P. Lau, *ACS Nano* **2012**, *6*, 5102.
[29] L. L. Li, J. Ji, R. Fei, C. Z. Wang, Q. Lu, J. R. Zhang, L. P. Jiang, J. J. Zhu, *Adv. Funct. Mater.* **2012**, *22*, 2971.
[30] Y. Li, Y. Zhao, H. H. Cheng, Y. Hu, G. Q. Shi, L. M. Dai, L. T. Qu, *J. Am. Chem. Soc.* **2012**, *134*, 15.
[31] Y. Q. Dong, C. Q. Chen, X. T. Zheng, L. L. Gao, Z. M. Cui, H. B. Yang, C. X. Guo, Y. W. Chi, C. M. Li, *J. Mater. Chem.* **2012**, *22*, 8764.
[32] D. Pan, J. Zhang, Z. Li, M. Wu, *Adv. Mater.* **2010**, *22*, 734.
[33] S. J. Zhu, S. J. Tang, J. H. Zhang, B. Yang, *Chem. Commun.* **2012**, *48*, 4527.
[34] J. Peng, W. Gao, B. K. Gupta, Z. Liu, R. Romero-Aburto, L. H. Ge, L. Song, L. B. Alemany, X. B. Zhan, G. H. Gao, S. A. Vithayathil, B. A. Kaipparettu, A. A. Marti, T. Hayashi, J. -J. Zhu, P. M. Ajayan, *Nano Lett.* **2012**, *12*, 844.
[35] Y. Qian, S. B. Lu, F. L. Gao, *J Mater Sci.* **2011**, *46*, 3517.
[36] M. Beidaghi, C. L. Wang, *Adv. Funct. Mater.* **2012**, *22*, 4501.
[37] K. X. Sheng, Y. Q. Sun, C. Li, W. J. Yuan, G. Q. Shi, *Sci. Rep.* **2012**, *2*, 247.
[38] X. Xiao, T. Q. Li, P. H. Yang, Y. Gao, H. Y. Jin, W. J. Ni, W. H. Zhan, X. H. Zhang, Y. Z. Cao, J. W. Zhong, L. Gong, W. -C. Yen, W. J. Mai, J. Chen, K. F. Huo, Y. -L. Chueh, Z. L. Wang, J. Zhou, *ACS Nano.* **2012**, *6*, 9200.
[39] W. Sun, X.Y. Chen, *J. Power Sources* **2009**, *193*, 924.
[40] J. -H. Sung, S. -J. Kim, S. -H. Jeong, E. -H. Kim, K. -H. Lee, *J. Power Sources* **2006**, *162*, 1467.
[41] M. Q. Xue, Z. Xie, L. S. Zhang, X. L. Ma, X. L. Wu, Y. G. Guo, W. G. Song, Z. B. Li, T. B. Cao, *Nanoscale* **2011**, *3*, 2703.
[42] Y. P. Fu, X. Cai, H. W. Wu, Z. B. Lv, S. C. Hou, M. Peng, X. Yu, D. C. Zou, *Adv. Mater.* **2012**, *24*, 5713.
[43] J. P. Alper, M. Vincent, C. Carraro, R. Maboudian, *Appl. Phys. Lett.* **2012**, *100*, 163901.
[44] M. D. Stoller, S. J. Park, Y. W. Zhu, J. H. An, R. S. Ruoff, *Nano Lett.* **2008**, *8*, 3498.
[45] Y. Wang, Z. Q. Shi, Y. Huang, Y. F. Ma, C. Y. Wang, M. M. Chen, Y. S. Chen, *J. Phys. Chem. C* **2009**, *113*, 13103.
[46] J. Li, H. Q. Xie, Y. Li, J. Liu, Z. X. Li, *J. Power Sources* **2011**, *196*, 10775.
[47] A. Izadi-Najafabadi, D. T. H. Tan, J. D. Madden, *Synth. Met.* **2005**, *152*, 129.
[48] A. Celzard, F. Collas, J. F. Mareche, G. Furdin, I. Rey, *J. Power Sources* **2002**, *108*, 153.
[49] Y. Honda, T. Haramoto, M. Takeshige, H. Shiozaki, T. Kitamura, M. Ishikawa, *Electrochem. Solid-State Lett.* **2007**, *10*, A106.
[50] Z. X. Li, J. Chen, *Microelectron. Eng.* **2008**, *85*, 1549.
[51] P. L. Taberna, P. Simon, J. F. Fauvarque, *J. Electrochem. Soc.* **2003**, *150*, A292.
[52] V. Presser, L. Zhang, J. J. Niu, J. McDonough, C. Perez, H. Fong, Y. Gogotsi, *Adv. Energy Mater.* **2011**, *1*, 423.
[53] X. Li, J. P. Rong, B. Q. Wei, *ACS Nano* **2010**, *4*, 6039.
[54] R. Z. Li, X. Ren, F. Zhang, C. Du, J. P. Liu, *Chem. Commun.* **2012**, *48*, 5010.
[55] X. Li, B. Q. Wei, *Nano Energy* **2012**, *1*, 479.
[56] Q. Gao, L. Demarconnay, E. Raymundo-Pineroa, F. Beguin, *Energy Environ. Sci.* **2012**, *5*, 9611.
[57] J. M. Shen, A. D. Liu, Y. Tu, G. S. Foo, C. B. Yeo, M. B. Chan-Park, R. R. Jiang, Y. Chen, *Energy Environ. Sci.* **2011**, *4*, 4220.
[58] Y. Gogotsi, P. Simon, *Science* **2011**, *334*, 917.
[59] J. J. Yoo, K. Balakrishnan, J. S. Huang, V. Meunier, B. G. Sumpter, A. Srivastava, M. Conway, A. L. M. Reddy, J. Yu, R. Vajtai, P. M. Ajayan, *Nano Lett.* **2011**, *11*, 1423.
[60] W. Gao, N. Singh, L. Song, Z. Liu, A. L. M. Reddy, L. J. Ci, R. Vajtai, Q. Zhang, B. Q. Wei, P. M. Ajayan, *Nat. Nanotechnol.* **2011**, *6*, 496.
[61] Jaidev S. Ramaprabhu, *J. Mater. Chem.* **2012**, *22*, 18775.
[62] X. Li, T. L. Gu, B. Q. Wei, *Nano Lett.* **2012**, *12*, 6366.
[63] M. F. El-Kady, V. Strong, S. Dubin, R. B. Kaner, *Science* **2012**, *335*, 1326.
[64] M. M. Jaramillo, A. Mendoza, S. Vaquero, M. Anderson, J. Palma, R. Marcilla, *RSC Adv.* **2012**, *2*, 8439.
[65] T. A. Centeno, M. Hahn, J. A. Fernandez, R. Kotz, F. Stoeckli, *Electrochem. Commun.* **2007**, *9*, 1242.
[66] W. W. Liu, X. B. Yan, J. W. Lang, Q. J. Xue, *J. Mater. Chem.* **2011**, *21*, 13205.
[67] Y. Chen, X. Zhang, D. C. Zhang, P. Yu, Y. W. Ma, *Carbon* **2011**, *49*, 573.
[68] W. W. Liu, X. B. Yan, J. W. Lang, Q. J. Xue, *J. Mater. Chem.* **2012**, *22*, 8853.
[69] S. Chen, J.W. Zhu, X. D. Wu, Q. F. Han, X. Wang, *ACS Nano* **2010**, *4*, 2822.
[70] R. R. Maphanga, D. C. Sayle, T. X. T. Sayle, P. E. Ngoepe, *Phys. Chem. Chem. Phys.* **2011**, *13*, 1307.
[71] M. Q. Wu, G. A. Snook, G. Z. Chen, *Electrochem. Commun.* **2004**, *6*, 499.
[72] Z. J. Fan, J. Yan, T. Wei, L. J. Zhi, G. Q. Ning, T. Y. Li, F. Wei, *Adv. Funct. Mater.* **2011**, *21*, 2366.
[73] C. -C. Lin, H. -W. Chen, *Electrochim. Acta* **2009**, *54*, 3073.
[74] Z. S. Wu, W. C. Ren, D. W. Wang, F. Li, B. L. Liu, H. M. Cheng, *ACS Nano* **2010**, *4*, 5835.
[75] X. L. Wang, H. Bai, G. Q. Shi, *J. Am. Chem. Soc.* **2011**, *133*, 6338.
[76] G. M. Zhou, D. W. Wang, X. Y. Shan, N. Li, F. Li, H. M. Cheng, *J. Mater. Chem.* **2012**, *22*, 11252.
[77] J. Yang, J. T. Chen, S. X. Yu, X. B. Yan, Q. j. Xue, *Carbon* **2010**, *48*, 2644.
[78] S. J. Zhu, J. H. Zhang, S. J. Tang, C. Y. Qiao, L. Wang, H. Y. Wang, X. Liu, B. Li, Y. F. Li, W. L. Yu, X. F. Wang, H. C. Sun, B. Yang, *Adv. Funct. Mater.* **2012**, *22*, 4732.
[79] S. J. Zhu, J. H. Zhang, X. Liu, B. Li, X. F. Wang, S. J. Tang, Q. N. Meng, Y. F. Li, C. Shi, R. Hu, B. Yang, *RSC Adv.* **2012**, *2*, 2717.